Evaluation of snowmelt simulation in the Weather Research and Forecasting model

Jiming Jin[1] and Lijuan Wen[1]

Received 5 October 2011; revised 20 March 2012; accepted 16 April 2012; published 25 May 2012.

[1] The objective of this study is to better understand and improve snowmelt simulations in the advanced Weather Research and Forecasting (WRF) model by coupling it with the Community Land Model (CLM) Version 3.5. Both WRF and CLM are developed by the National Center for Atmospheric Research. The automated Snow Telemetry (SNOTEL) station data over the Columbia River Basin in the northwestern United States are used to evaluate snowmelt simulations generated with the coupled WRF-CLM model. These SNOTEL data include snow water equivalent (SWE), precipitation, and temperature. The simulations cover the period of March through June 2002 and focus mostly on the snowmelt season. Initial results show that when compared to observations, WRF-CLM significantly improves the simulations of SWE, which is underestimated when the release version of WRF is coupled with the Noah and Rapid Update Cycle (RUC) land surface schemes, in which snow physics is oversimplified. Further analysis shows that more realistic snow surface energy allocation in CLM is an important process that results in improved snowmelt simulations when compared to that in Noah and RUC. Additional simulations with WRF-CLM at different horizontal spatial resolutions indicate that accurate description of topography is also vital to SWE simulations. WRF-CLM at 10 km resolution produces the most realistic SWE simulations when compared to those produced with coarser spatial resolutions in which SWE is remarkably underestimated. The coupled WRF-CLM provides an important tool for research and forecasts in weather, climate, and water resources at regional scales.

Citation: Jin, J., and L. Wen (2012), Evaluation of snowmelt simulation in the Weather Research and Forecasting model, *J. Geophys. Res.*, *117*, D10110, doi:10.1029/2011JD016980.

1. Introduction

[2] In the western United States (WUS), maximum precipitation occurs in the cold seasons, and minimum precipitation falls in the warm seasons. This bimodality leads 50–70% of the annual precipitation in this mountainous region to falling as snow [*Serreze et al.*, 1999], resulting in 75–85% of the annual streamflow coming from snowmelt runoff [*Grant and Kahan*, 1974]. Fossil fuel emissions have caused a 1°C increase in global temperature during the last 100 years, with an additional 2–5°C temperature increase anticipated by the end of this century [*Intergovernmental Panel on Climate Change*, 2008]. Snow is especially vulnerable to such climate change. By analyzing more than 50 year observations, *Knowles et al.* [2006] found that more precipitation falling as rain instead of snow and earlier-than-normal snowmelt in the WUS can be attributed to warming across the region. Thus, accurate predictions of snow mass in the WUS are crucial to the region's well-being under the current climate change background. Efforts to better understand and more accurately predict snow mass in the WUS have been made by a number of researchers through observational analysis and numerical modeling (e.g., *McCabe and Wolock* [1999], *Mote* [2003], *Leung and Qian* [2003], *Jin et al.* [2006], and many others). These efforts have significantly advanced the ability to predict snow mass in the WUS.

[3] Large-scale atmospheric processes have a significant influence on snow in the WUS. Research has indicated that about 20% or less of the snow mass variance in the WUS results from shifts in air moisture transport caused by the El Niño–Southern Oscillation [*McCabe and Dettinger*, 2002; *Jin et al.*, 2006]. *Jin et al.* [2006] also found that the internal variability of the atmosphere contributes significantly to the snow variance in this region. *Lo and Clark* [2002] indicated that an inverse correlation exists between WUS wintertime mountain snow and the North American summer monsoon rainfall, implying that seasonal variations of snow in the WUS are closely related to the summer surface heating processes that alter the atmospheric circulation and precipitation. In addition, the mountainous topography in the WUS complicates the spatial distribution of snow. Under a warming background, snow has a most pronounced decrease at lower and middle elevations, while observed absolute temperatures at higher elevations are still sufficiently low that a large

[1]Department of Watershed Sciences and Department of Plants, Soils, and Climate, Utah State University, Logan, Utah, USA.

Corresponding author: J. Jin, Department of Watershed Sciences, Utah State University, 5210 Old Main Hill, Logan, UT 84322-5210, USA. (jiming.jin@usu.edu)

0148-0227/12/2011JD016980

Table 1. Comparison of the Noah, RUC, and CLM Land Surface Schemes in WRF

Model	Vegetation	Soil	Snow
CLM	Subgrids with up to 10 vegetation types in one grid cell	10-layer temperatures and moistures and frozen soil	5-layer snow with liquid water; variable snow density
Noah	One vegetation type in one grid cell	4-layer temperatures and moistures and frozen soil	1-layer snow lumped with the topsoil layer; no liquid water; fixed snow density
RUC	One vegetation type in one grid cell	6-layer temperatures and moistures and frozen soil	2-layer snow; no liquid water; fixed snow density

decrease of snow mass is not apparent [*McCabe and Clark*, 2005]. *Howat and Tulaczyk* [2005] indicated that the snow mass in the WUS even showed an upward trend on the tops of some WUS mountains, a result of amplified cold season precipitation. This amplified precipitation at higher elevations is caused by strong orographic lifting of air with larger water-holding capacity under a warming climate condition. Thus, snow predictions could be improved if the topography were more accurately described in the numerical computer models [*Leung and Qian*, 2003] that have played an important role in snow and related hydroclimate research and forecasts.

[4] Recent development of numerical computer models has led to improvement in snow research and forecasts [*Livneh et al.*, 2010; *Jin and Miller*, 2007; *Wang et al.*, 2010; *Leung and Qian*, 2003; *Rauscher et al.*, 2008]. However, process level mechanisms and parameterizations related to snow predictability have not been adequately addressed in both dynamically coupled weather and climate models and off-line snow models, and large uncertainties still exist in these models. These uncertainties include the errors in atmospheric forcings and oversimplified snow physics and model structure. This study focuses on the improvement of snow simulations in a state-of-the-art next generation regional climate model by coupling it with a more sophisticated snow model. Using this coupled model, detailed physical processes and mechanisms that control snow simulations are quantified, and the impact of snow on critical weather and climate variables such as temperature and precipitation is described. Section 2 introduces the model and provides the data description and methodology for this study, section 3 provides the modeling results and comparisons to observations, and section 4 gives a discussion and conclusions.

2. Model, Methodology, and Data

[5] The regional climate model used in this study is Version 3.0 of the Weather Research and Forecasting (WRF) model developed by the National Center for Atmospheric Research (NCAR). We recently coupled the advanced Community Land Model (CLM) Version 3.5 with WRF to improve regional climate simulations [*Jin et al.*, 2010; *Subin et al.*, 2011]. We have performed a series of simulations with different combinations of the physical schemes within WRF coupled with CLM over the WUS at 10 km resolution and have found an optimal combination that produces realistic precipitation and temperature simulations (see section 3). In this optimal combination, the microphysics scheme selected was the WRF Single-Moment 3 class (WSM3) scheme [*Hong et al.*, 2004]. The Mellor-Yamada-Janjic scheme was used for the boundary layer processes [*Janjic*, 1996], and the Grell-Dévényi ensemble convection scheme [*Grell and Dévényi*, 2002] was used to parameterize cumulus clouds. The Rapid Radiative Transfer Model (RRTM) based on *Mlawer et al.* [1997] was selected for calculating longwave radiation, and the Goddard shortwave scheme was used for calculating shortwave radiation [*Chou and Suarez*, 1999].

[6] To better understand the simulations of snow and related processes, WRF-CLM simulations were compared with those from WRF coupled with the Noah [*Barlage et al.*, 2010; *LeMone et al.*, 2010a, 2010b] and Rapid Update Cycle (RUC) [*Smirnova et al.*, 1997, 2000; *McKeen et al.*, 2005] land surface schemes. The Noah and RUC land surface schemes were originally embedded in the release version of WRF. The comparison of the three land surface schemes is shown in Table 1. CLM has been shown to be accurate in describing snow, soil, and vegetation processes for global and regional applications [*Bonan et al.*, 2002; *Zeng et al.*, 2002; *Jin and Miller*, 2007]. CLM includes a five-layer snow scheme, a 10-layer soil scheme, and a single-layer vegetation scheme. Solid ice and liquid water are described in the snowpack as prognostic variables. A sophisticated snow compaction scheme is used to calculate the height and density of snow, where snow density is a critical variable for describing the water and heat transfer within the snowpack [*Jin et al.*, 1999a]. The model physically describes frozen soil processes and their impact on soil properties. The two-stream approximation [*Dickinson*, 1983; *Sellers*, 1985] is applied to the vegetation to calculate solar radiation reflected and absorbed by the canopy as well as its transfer within the canopy. A maximum of 10 subgrids per model grid is included in CLM to better represent subgrid heterogeneity of the land surface. The 24 United States Geological Survey (USGS) land use types are translated to the 16 plant functional types in CLM based on a lookup table. The soil is divided into 19 categories defined as percentages of sand and clay. Additional technical details on CLM are provided in *Oleson et al.* [2004].

[7] As shown in Table 1, Noah has four soil layers, with a total depth of two meters and a single slab snow layer lumped with the topsoil layer, which is set to 10 cm. Although the vegetation is separated from the soil in Noah, the heat and water fluxes between the bottom of the canopy and the soil/snow surface are not described. In addition, Noah does not have subgrid cells within its model grid cell. Unlike Noah, RUC has two separate snow layers, which is different from Noah, but the structure and physics of these two models are generally quite similar. In particular, the vegetation scheme in RUC [*Smirnova et al.*, 1997] is taken from that in *Pan and Mahrt* [1987], which is also used in Noah. In addition, liquid water transfer in the snowpack is missing in both Noah and RUC, but is included in CLM. This transfer is important to snowpack simulations and was discussed in detail in *Jin et al.* [1999a].

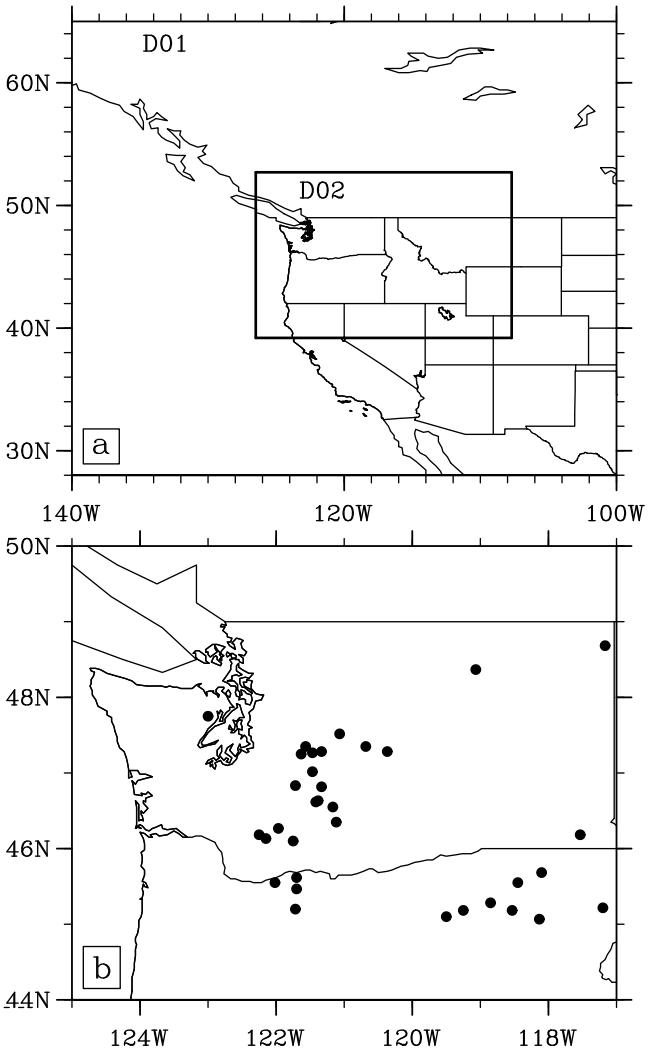

Figure 1. (a) The nested domains in WRF. D01 is the 30 km resolution domain, and D02 is the 10 km resolution domain. (b) The geographical distribution of the 32 SNOTEL stations (black dots).

[8] A series of WRF nested simulations was performed with the three land surface schemes. These nested simulations included two-way 30 km (domain D1) to 10 km (domain D2) resolutions (Figure 1a). The 30 km resolution domain (D1) covered the WUS, parts of the eastern Pacific Ocean, and western Canada. The nested 10 km resolution domain (D2) covered the Pacific Northwest, including the entire Columbia River Basin, where snow is the main water resource and is the focus of this analysis. Additional WRF-CLM simulations were performed with 180–60 km, 90–30 km, and 60–20 km nested domains to examine how and to what extent model resolutions affect snow simulations. In these additional simulations, the model physics options and domain sizes were the same. Only the results from the inner domains (60, 30, 20, and 10 km) are analyzed. The WRF is configured with 28 vertical sigma layers from the surface to the 100 hPa level for all simulations in order to capture physical processes within the planetary boundary layer and the upper atmosphere. There is no adjustment made for the default model parameters related to snow in CLM, Noah, and RUC, and those default parameters are used for all simulations generated in this study. The National Centers for Environmental Prediction/NCAR (NCEP/NCAR) Reanalysis data at 2.5° × 2.5° resolution were used as WRF initial and lateral boundary conditions. The latter were updated every 6 h over the period of 2 March through 30 June 2002, a period that is under neutral tropical Pacific sea surface temperature conditions. Across the WUS, snow usually reaches its maximum amount around 1 April [*Serreze et al.*, 1999] and then starts to melt. Thus, in our study period, snowmelting was the major process.

[9] The main focus of this study is evaluating the snowmelt schemes in the three land surface models coupled with WRF. However, the current release versions of WRF overestimate winter precipitation especially over the mountainous the WUS as described in *Jin et al.* [2010], which is likely to lead to overestimated snowpack. In this case, even a perfect snow scheme would be unable to produce a realistic snowpack simulation because of the overestimated precipitation. To avoid this problem, we chose the spring and early summer (March through June) for our study period, a time when WRF produces reasonable precipitation simulations (discussed in section 3). In addition, most precipitation falls as rain instead of snow during this period of time, which significantly reduces the impact of precipitation on snowpack simulations and allowed us to fully evaluate the reliability of the snow schemes in WRF.

[10] The observed Snow Telemetry (SNOTEL) data included daily snow water equivalent (SWE), 2 m height temperature, and precipitation (used here for model evaluation), which were quality controlled using the method described in *Serreze et al.* [1999]. Observations were taken from 32 selected SNOTEL stations (Figure 1b), all of which were located in Washington and northern Oregon. The observed SNOTEL SWE values were also used for model initialization in both the 30 km and 10 km resolution domains at the corresponding grid cells, because of the poor quality of the NCEP/NCAR reanalyzed SWE data. For the model grid cells without available SNOTEL SWE data, the 0.125° × 0.125° girded SWE data produced by the North American Land Data Assimilation System [*Pan et al.*, 2003] were used for the initial conditions. Thus, in the grid cells where the SNOTEL stations exist, the SWEs were initialized with the observations from the 32 SNOTEL stations located in the Columbia River Basin (Figure 1b).

3. Results

3.1. Snow Simulations

[11] WRF runs with CLM, Noah, and RUC land surface schemes were performed to examine snowpack simulations over the Columbia River Basin. Figure 2a shows the time series of observed and simulated SWE averaged over the 32 SNOTEL stations in the Columbia River Basin with the three land surface schemes in WRF at 10 km resolution. The results at other resolutions are analyzed in section 3.4. It is clear that CLM can accurately reproduce the observed snowpack, while Noah and RUC dramatically underestimate it. The averaged SWE over the study period for observation is 494 mm, and for CLM, it is 511 mm (Table 2). CLM slightly overestimates the SWE in March (Figure 2a). The averaged SWE for Noah for our study period is 174 mm, and for RUC,

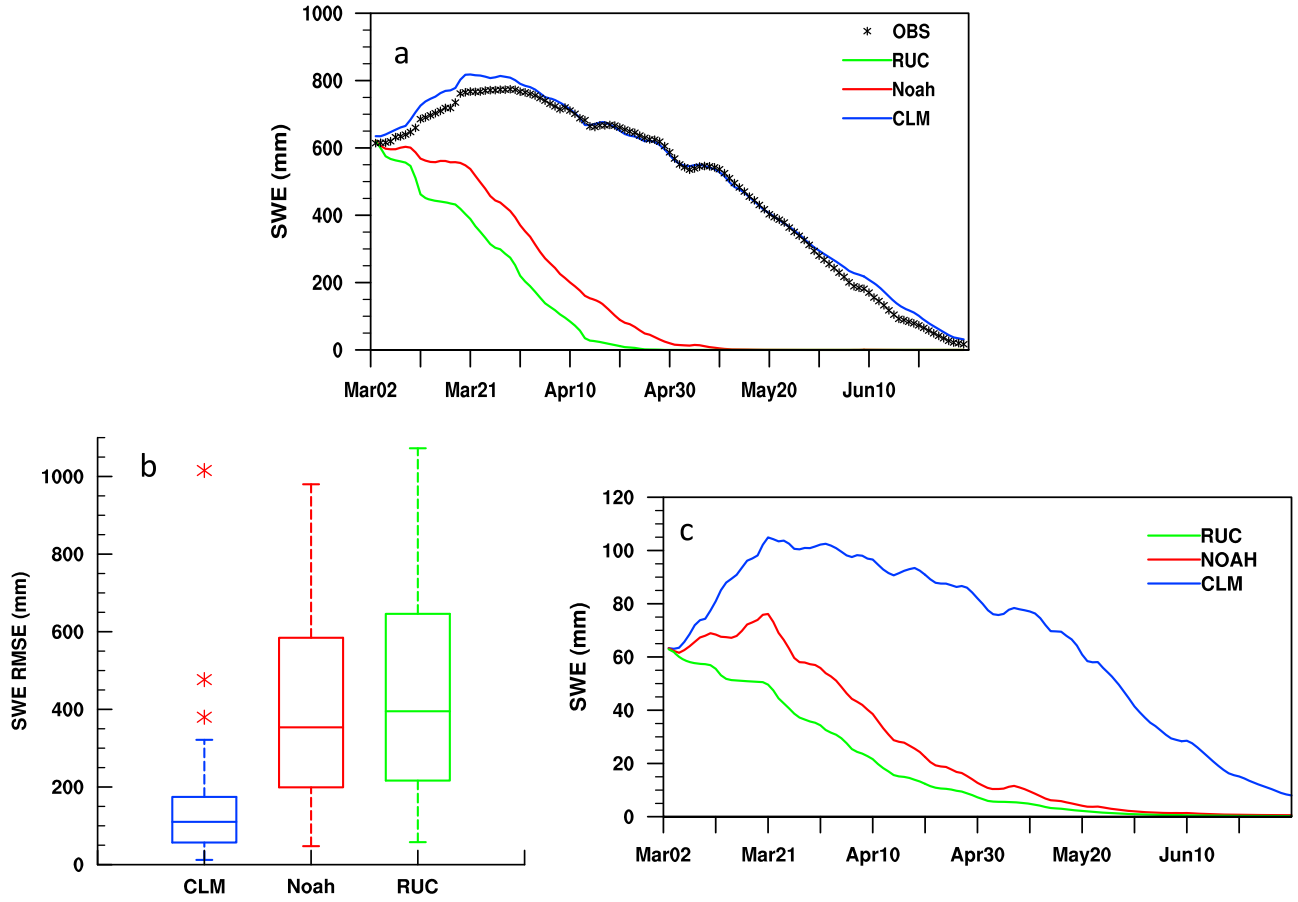

Figure 2. (a) SWE observations and simulations of WRF with CLM, Noah, and RUC averaged over the 32 SNOTEL station stations for the period of 2 March through 30 June 2002. (b) The box plots of the SWE RMSE for CLM (blue), Noah (red), and RUC (green). The whiskers represent the minimum and maximum values, and the stars represent the outliers. (c) The domain-averaged SWE at 10 km resolution for these three land surface models for the same period.

it is 123 mm. Obviously, the simulated SWE values in both Noah and RUC are considerably lower than the observations and those in CLM.

[12] Figure 2b shows the root-mean-square errors (RMSEs) for SWE with a box plot for the 32 SNOTEL stations. CLM generally has the lowest errors and the smallest interquartile range (IQR, the box height), although it generates outliers at three stations, indicating that CLM's performance is consistent at most of the 32 SNOTEL stations. The time series of the domain-averaged SWE at 10 km resolution demonstrates a similar pattern to that for the SNOTEL stations (Figure 2c), indicating that the temporal evolution of SWE at the SNOTEL stations is representative for the entire domain. Figure 3 illustrates the spatial distribution of the SWE biases from the three land surface schemes. Obviously, the largest errors occur in the Cascade Range (near the west coast region) for all schemes, and the most dramatic negative biases are seen in Noah and RUC. It is also found that the observed maximum SWE averaged over the 20 stations west of 120°W is nearly 1,000 mm, while it is only 500 mm averaged over the 12 inland stations east of 120°W. However, the time series of the simulated SWE and their biases both in the Cascades and inland still follow a similar pattern, shown in Figure 2a. The large errors in the Cascades are related to the large absolute SWE values there. For instance, 10% of the error in the simulated SWE in the Cascades is about 100 mm, while it is 50 mm inland.

[13] In these WRF simulations, all the model settings are exactly the same except for land surface scheme. Thus, it is quite obvious that the differences in the SWE simulations are caused by the land surface schemes.

3.2. Surface Energy Allocation in CLM, Noah, and RUC

[14] As discussed in section 2, CLM3 has up to 10 subgrids in one model grid cell. Such a subgrid configuration is not included in Noah or RUC. These subgrids lead to a significant difference in surface energy allocation as compared with those models without them, especially over highly

Table 2. The Mean Observations and Simulations From WRF With CLM, Noah, and RUC Over the 32 SNOTEL Stations for 2 March Through 30 June 2002

	OBS	CLM	Noah	RUC
SWE (mm)	494	511	174	123
Temperature (°C)	3.5	4.1	4.4	5.1
Precipitation (mm/d)	3.9	5.0	5.8	5.5

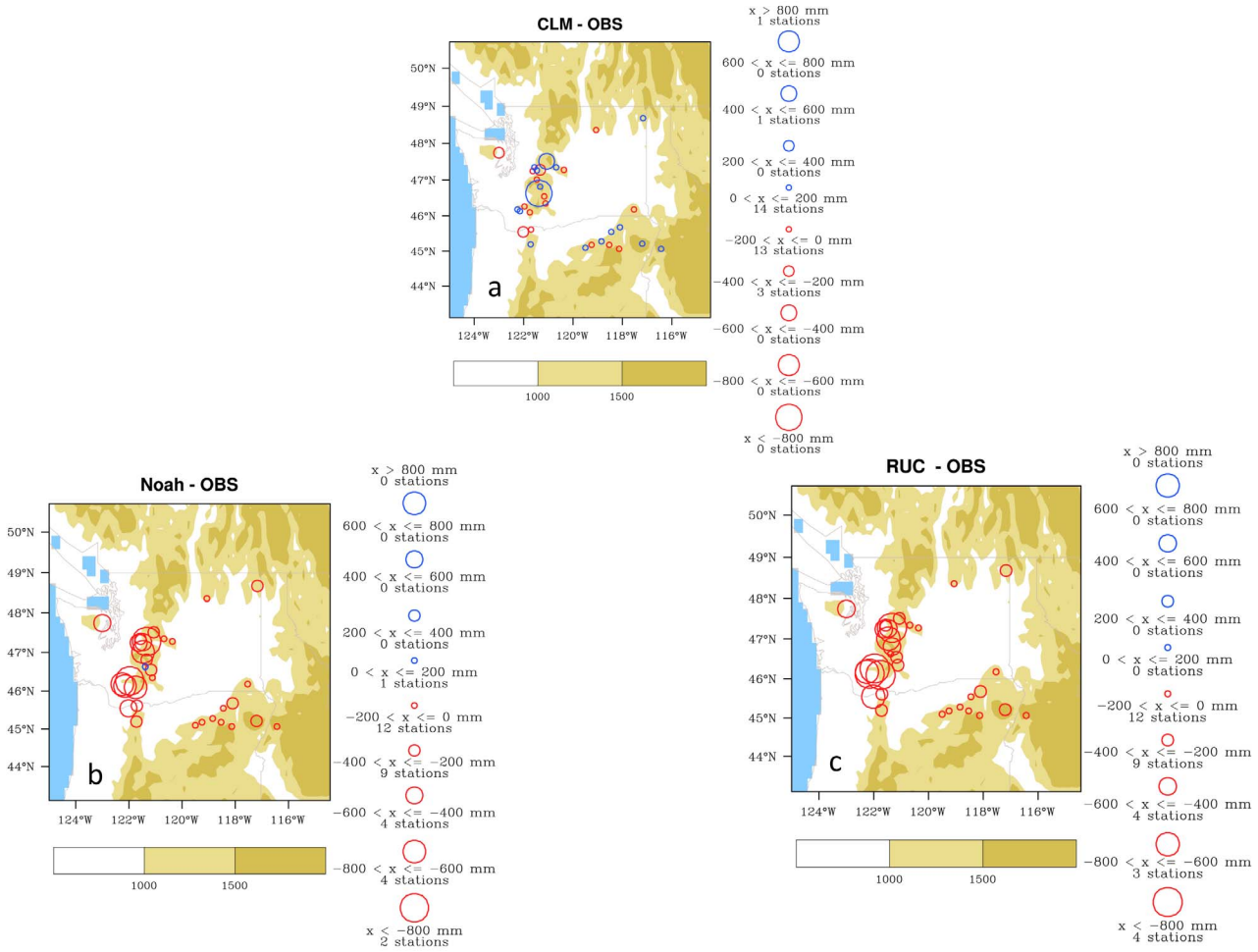

Figure 3. Spatial distribution of SWE biases for the 32 SNOTEL stations from the 10 km resolution results for (a) CLM, (b) Noah, and (c) RUC. The blue circles represent positive biases, and the red circles represent negative biases. The number of stations for each bias range is shown in the legends.

heterogeneous surfaces. In both Noah and RUC, the following energy balance equation is used for computing the snowmelt [*Chen and Dudhia*, 2001; *Smirnova et al.*, 2000]:

$$(1-\alpha_g)S_g\downarrow + (LWD_a - LWU) - H - LE - G - H_m = 0, \quad (1)$$

where α_g is the albedo of the grid cell, which includes the effects of snow, soil, and vegetation, $S_g\downarrow$ is the downward solar radiation for the grid cell, LWD_a is the downward longwave radiation from the atmosphere, LWU is the longwave emission from the snow/soil surface, H is the sensible heat flux, LE is the latent heat flux (where L is the latent heat of vaporization ($2.5\ e^6$ J kg^{-1}), and E is evaporation), G is the ground heat flux, and H_m is the heat flux used to melt the snow. However, in CLM, a different energy balance equation is used to estimate the snowmelt [*Oleson et al.*, 2004]:

$$(1-\alpha_s)S_o\downarrow + (LWD_{a+v} - LWU) - H - LE - G - H_m = 0, \quad (2)$$

where α_s is the snow/soil surface albedo, $S_o\downarrow$ is fractional downward solar radiation to the surface for the open area in the model grid cell, and LWD_{a+v} is the downward longwave radiation from the atmosphere and the canopy bottom to the surface.

[15] It is noteworthy that the entire downward solar radiation ($S_g\downarrow$) in equation (1) is used for calculating the heat flux for melting snow, which is reasonable if the snow surface in the model grid cell of a land surface model is exposed to the air without vegetation coverage. Surface albedo is used to calculate net solar radiation.

[16] However, a problem emerges if there are snow and vegetation coexisting in a model grid cell. In this case, part of the downward solar radiation is intercepted by the vegetation, and the rest of the solar radiation can reach the snow surface if it is not fully covered by the vegetation. If the entire downward solar radiation is still used to estimate the snowmelt flux as shown in equation (1), a faster snowmelt could occur. In addition, the grid cell albedo (α_g) should be an area-weighted average of vegetation and snow surface albedos when only these two land use types coexist. This albedo is usually lower than the albedo of snow alone, which could

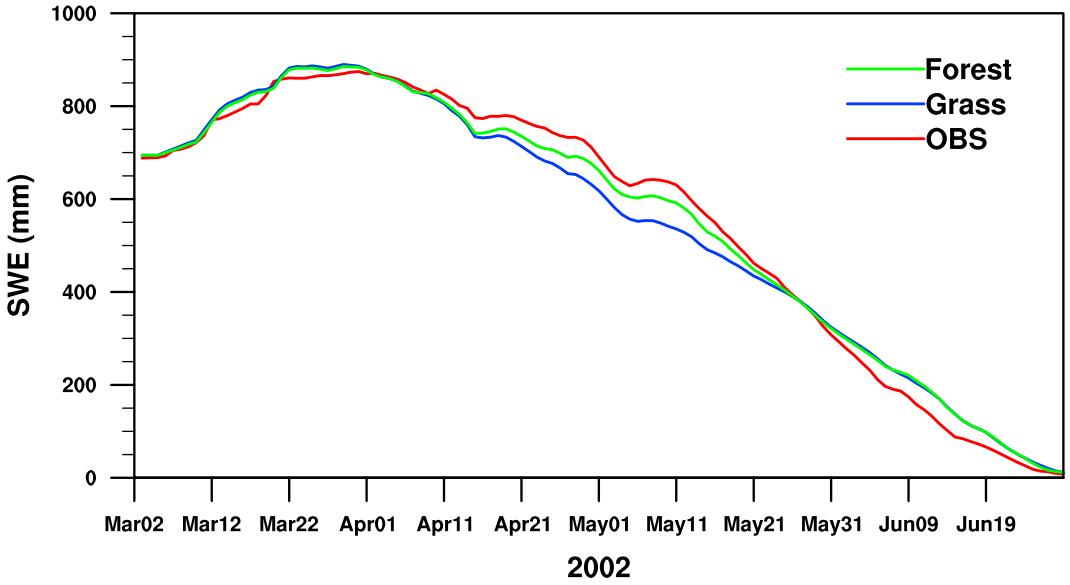

Figure 4. The SWE observations and simulations with WRF-CLM for the period of 2 March through 30 June 2002. The green line represents the SWE simulations averaged over the 26 SNOTEL stations covered by forest, and the blue line represents those averaged over the same SNOTEL stations, but their land use type is changed to grassland.

further increase snow surface temperature or intensify snowmelt in Noah and RUC.

[17] However, a CLM grid cell includes subgrids that could lead to more reasonable surface energy allocation over a heterogeneous surface, as in equation (2). When snow coexists with vegetation in one CLM grid cell, a fractional downward solar radiation ($S_o\downarrow$) is assigned to the snow surface exposed to the air according to the area weight, where snow albedo (α_s) is used for computing surface solar radiation absorption. For the snow directly under the canopy, solar radiation can still penetrate into the canopy and reach the snow surface according to a two-stream solar penetration scheme [*Dickinson*, 1983; *Sellers*, 1985]. The amount of incoming solar radiation reaching the surface is largely determined by the canopy leaf density (leaf area index) in CLM. At the same time, energy exchanges between the canopy bottom and the surface, such as longwave radiation and sensible and latent heat fluxes, are explicitly calculated. These CLM configurations more closely represent actual conditions than those in Noah and RUC. Therefore, realistic surface energy allocation is one of the important processes that lead to the improvement in CLM SWE simulations when compared to those in Noah and RUC under the same atmospheric model settings (Figure 2a). A similar discussion was also included in *Jin and Miller* [2007]. The vegetation effects on snow are analyzed again in the next section.

3.3. Effects of Vegetation on Snow Simulations

[18] In the WUS, almost all the SNOTEL stations where the SWEs were measured are located in open areas. Among our selected SNOTEL stations, 26 are located in the forest, and 6 stations are in grasslands. Those in the forest are still located in the open spaces between the trees. Thus, the SWE under the canopy is not measured. However, the SWE in a CLM grid cell with a forest land use type is an areal average of the SWE values under and outside the canopy. This model configuration indicates that the canopy sheltering effects are included in the simulated SWE in CLM. There seems to be an inconsistency between the simulations and observations. Nevertheless, it is clear from Figure 2a that the simulated SWE values in CLM agree very well with those that were measured over the open spaces as indicated above. Our reasoning process is as follows: all the SNOTEL stations selected for this study are located in the areas north of 45°N. Thus, during the snow season, the incoming solar radiation is mostly tilted toward the surface, and the snow surface outside the canopy, where the SNOTEL instruments are situated, is often shaded by the trees during the daytime, and not all the direct solar radiation can reach the surface. Therefore, canopy sheltering effects may be included in the measurements at our selected SNOTEL stations.

[19] In order to verify our speculation, one additional simulation with WRF-CLM was performed, where the forest land use type in those grid cells with SNOTEL stations (26 stations as mentioned above) was changed to the grassland (hereafter "Grass case"), and the other model settings remained the same as those in the WRF-CLM simulations shown in Figure 2 (hereafter "Forest case"). Doing this removes the canopy sheltering effects when the snow depth (not SWE) is higher than the grass height, which is set to 50 cm in CLM. Interestingly, Figure 4 shows that a faster SWE melting in the Grass case is seen only between late April and early May 2002 when compared to that in the Forest case with sheltering effects, and there is no significant difference in SWE between the two cases during the other times in our simulation period. However, when the snow duration at individual SNOTEL stations is examined (Figure 5), the snow duration in the Forest case is found to be generally longer than that in the Grass case when the simulated peak SWE (the average of the peak SWEs in the two cases at each SNOTEL station) is lower with some exceptions, and the largest duration difference can reach 16 days.

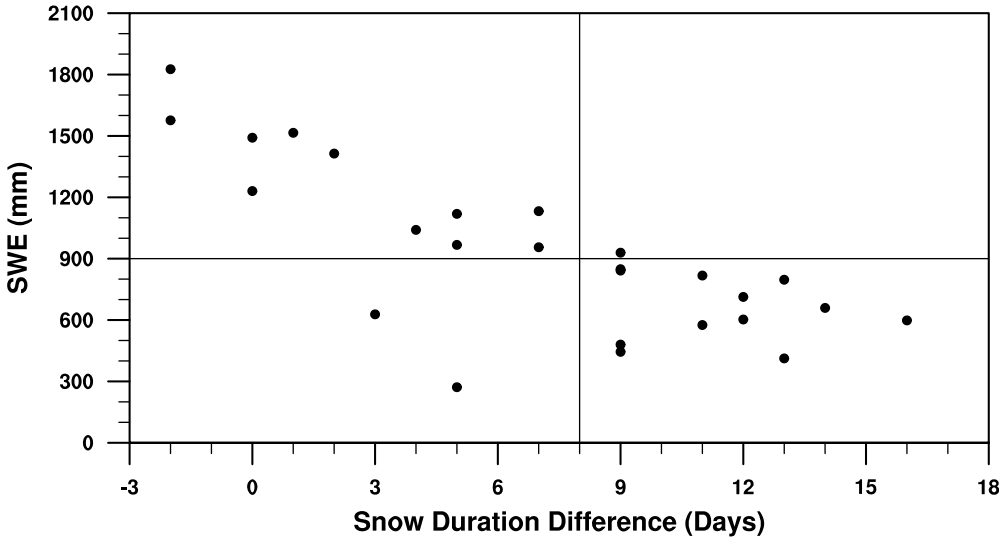

Figure 5. The snow duration difference (the Forest case – the Grass case) versus the peak SWE value that is an average over the Forest and Grass cases. The vertical line is for the 8 day duration difference, and the horizontal line is for the 900 mm SWE, which are discussed in the text.

[20] It is found that the snow duration difference between the Forest case and the Grass case is fewer than 8 days (the vertical line in Figure 5) when the peak SWE averaged over the two cases is higher than 900 mm (the horizontal line in Figure 5, although there are two exceptions), which is defined as "HPS" (high peak SWE). At the same time, the duration difference is more than 8 days when the peak SWE is lower than 900 mm (with one exception), which is defined as "LPS" (low peak SWE). These three exceptions are most likely linked to poor SWE simulations over the complex terrain area. The criterion used here (the 8 day snow duration difference) to categorize HPS and LPS is an arbitrary selection, but it appears to work reasonably well in the following analysis. The SWE values in Figure 6a are averaged over those SNOTEL stations (13 out of 26 stations) where the snow duration in the Forest case is 8 days longer than in the Grass case (for the LPS); the SWE values averaged over the rest of the stations are shown in Figure 6b (for the HPS). In Figure 6a, the simulated peak SWE values in the Forest and Grass cases are about 650 mm and are close to the observation, while such values are nearly doubled in Figure 6b. In general, a notably faster snowmelt in the Grass case is seen for the LPS, while for the HPS, there is no significant difference in snowmelt between the Forest and Grass cases.

[21] Figure 7 indicates that the surface (snow and/or soil) in the Grass case generally has stronger solar radiation absorption than in the Forest case during the snowmelt season, but the difference becomes smaller when the SWE increases. This phenomenon can be well explained by the relationship among snow fraction, SWE, and albedo [*Oleson et al.*, 2004; *Niu and Yang*, 2007]. A high SWE leads to a large snow fraction, resulting in a high surface albedo. The high albedo produces weak surface solar absorption, which can be analogous to the sheltering effects in the Forest case where the surface net solar radiation is reduced due to direct solar radiation to the surface being blocked by the trees. On the other hand, due to the effects of snow fraction in CLM, a low peak SWE results in a low albedo, resulting in stronger surface solar radiation absorption in the Grass case than in the Forest case (Figure 7) and generating a faster snowmelt (Figure 6b).

[22] It is noteworthy that the snowmelting rates in the Forest case are close to those in the Grass case under the HPS conditions (as shown in Figure 6b) even though the solar radiation absorption in the Grass case is 40–60 Wm^{-2} stronger than in the Forest case. This implies that the magnitudes of the total surface energy absorption should be similar in these two different land use type cases. Further examination indicates that under the HPS conditions the energy absorption deficit in the Forest case ($\sim$40–60 Wm^{-2}) is approximately compensated for by the stronger longwave radiative forcing from the bottom of the canopy, which is stronger than that coming mostly from the atmosphere in the Grass case (not shown).

[23] The above analysis clearly shows that the canopy sheltering effects need to be taken into account in WRF-CLM in order to reproduce the SNOTEL SWE observations. Although the snowmelt rates are similar for the cases with and without canopy sheltering under the HPS conditions due to the effects of albedo, such rates are significantly different under the LPS conditions. This discussion further verifies that the SWE measurements include the sheltering effects in the forests of our study region. If the model fails to consider such effects, simulated snowmelt will be faster than the observation. These modeling results need to be further evaluated with more detailed in situ observations. *Andreadis et al.* [2009] used high-quality SWE measurements taken beneath the canopy and in a nearby clearing at a site near the Oregon coast to study how vegetation cover affects the SWE. They found that the beneath-canopy SWE was significantly lower than that in the clearing due to the high-canopy interception of snow during the snow accumulation period, In this coastal area, the snowfall often contains a

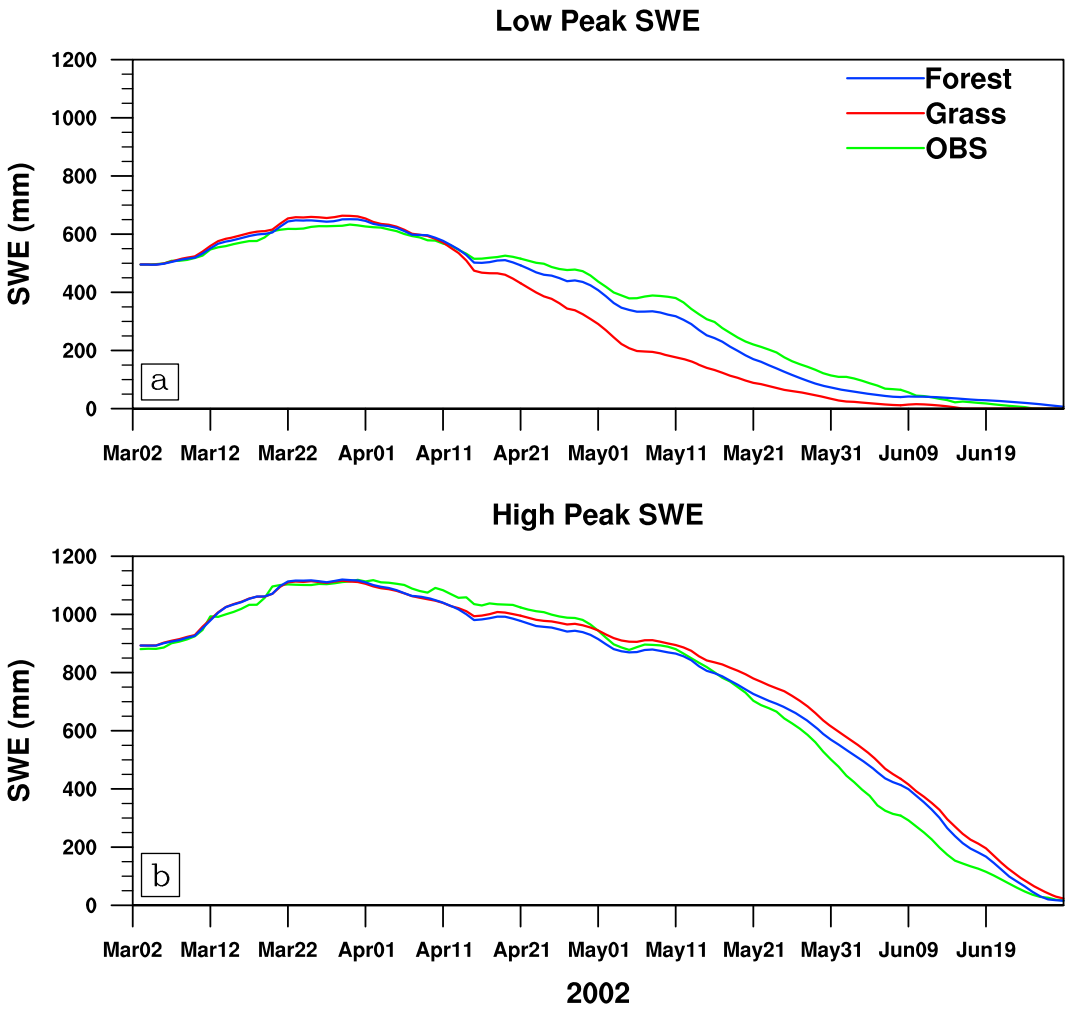

Figure 6. The averaged observations and simulations for the period of 2 March through 30 June 2002 for (a) LPS and (b) HPS.

high amount of liquid water that can easily adhere to the vegetation. However, in this study, many SNOTEL stations were located in the inland area where the liquid water content in the snowfall is likely to be lower. In addition, the main focus in this study is the snowmelt season during which rainfall is more dominant than snowfall. In this season, canopy snow interception processes would be unlikely to meaningfully affect the SWE on the ground. Thus, the conclusions drawn from *Andreadis et al.* [2009] may not apply to the snow canopy interactions at the SNOTEL stations selected for this study.

[24] It is also seen that vegetation apparently does not affect snowmelt as dramatically as it does using CLM, Noah, and RUC, where the latter two schemes do not include a canopy sheltering effect. In fact, *Jin and Miller* [2007] showed that such an effect results in a difference in snow duration of about two months between the cases with and without a canopy over the Sierra Nevada and is much stronger than that simulated in this study. The key reason is that the efficiency of the canopy sheltering effect is highly correlated with the intensity of incoming solar radiation. The data obtained from the United States National Renewable Energy Laboratory show that incoming solar radiation is about 25% stronger in the Sierra Nevada than in the Colombia River Basin on average over our study period, indicating that the canopy sheltering effect is more efficient in the former area than in the latter. In addition, snowmelt simulations are strongly affected by other factors such as model layering, liquid water transfer within the snowpack, or snow density. Those factors in the three land surface schemes within WRF are compared in the fourth column of Table 1, and more detailed discussions of the impact of model structure and physics on snowmelt are summarized in *Jin et al.* [1999a, 1999b], *Sun et al.* [1999], and *Jin and Miller* [2007], which are not reiterated in this study.

3.4. Precipitation and Temperature Simulations

[25] WRF with the three land surface schemes overestimated precipitation by more than 1 mm/d averaged over the 32 SNOTEL stations for the period of 2 March through 30 June 2002 (Figure 8a and Table 2). The averaged value of precipitation for observations is 3.9 mm/d, but for CLM, Noah, and RUC, they are 5.0, 5.8, and 5.5 mm/d respectively. Based on the box plot (Figure 8b), CLM also produces the lowest median value of the RMSEs (CLM: 7.0 mm/d; Noah: 7.5 mm/d; RUC: 7.2 mm/d). Moreover, the bias spatial

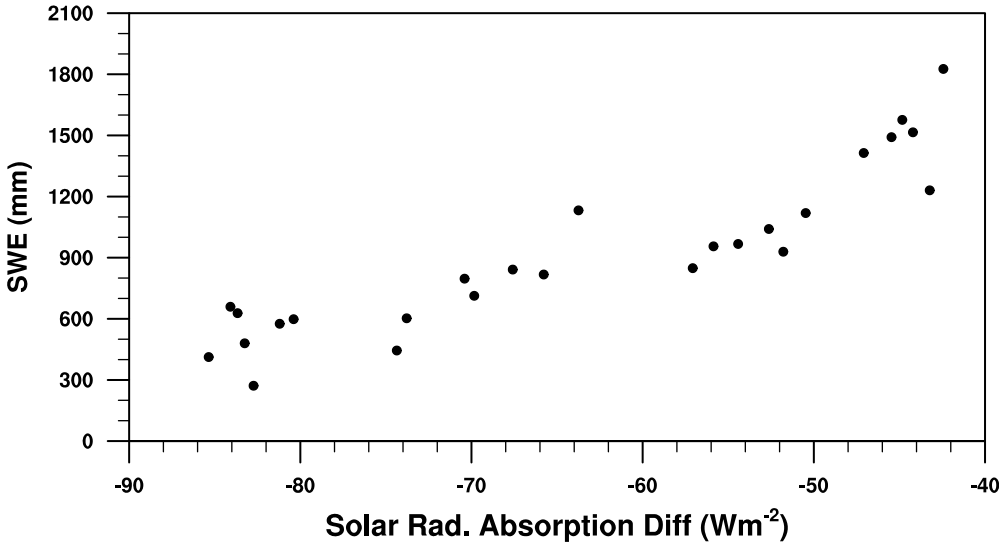

Figure 7. The peak SWE (vertical axis) versus the surface solar radiation difference between the Forest and Grass cases (Forest – Grass) (horizontal axis) averaged over April, May, and June of 2002.

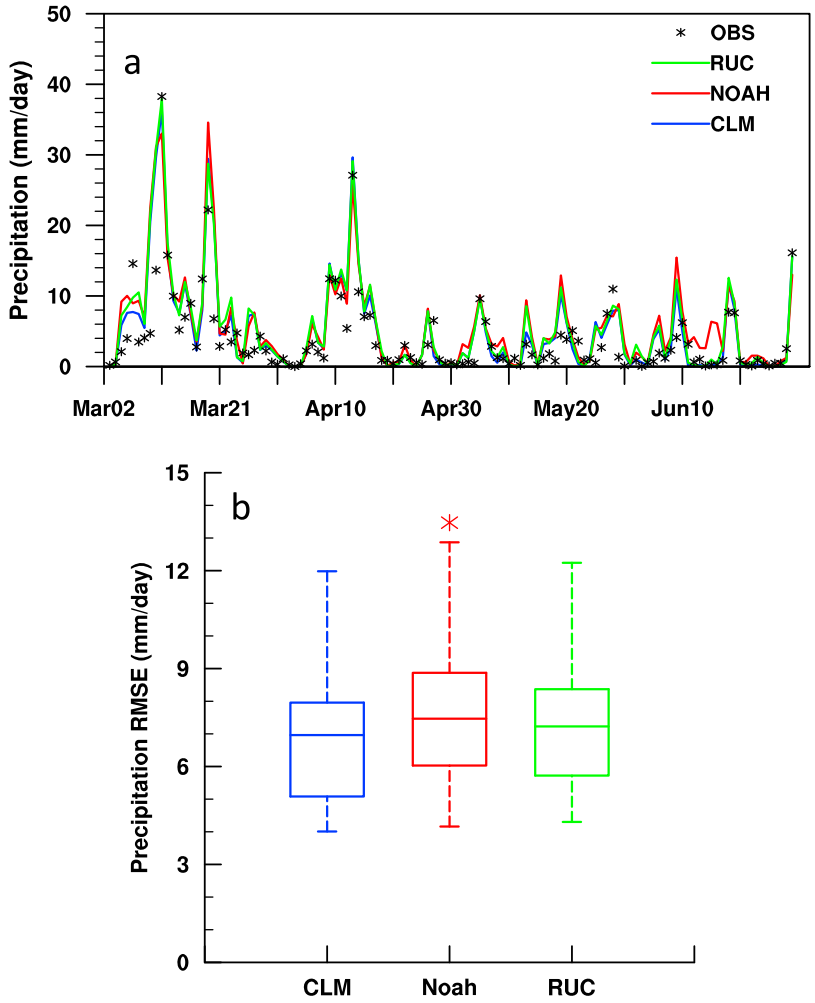

Figure 8. (a) Precipitation observations and simulations with WRF coupled with CLM, Noah, and RUC averaged over the 32 SNOTEL stations for the period of 2 March through 30 June 2002. (b) Box plots of the precipitation RMSE for CLM (blue), Noah (red), and RUC (green). The whiskers represent the minimum and maximum values, and the star represents the outliers.

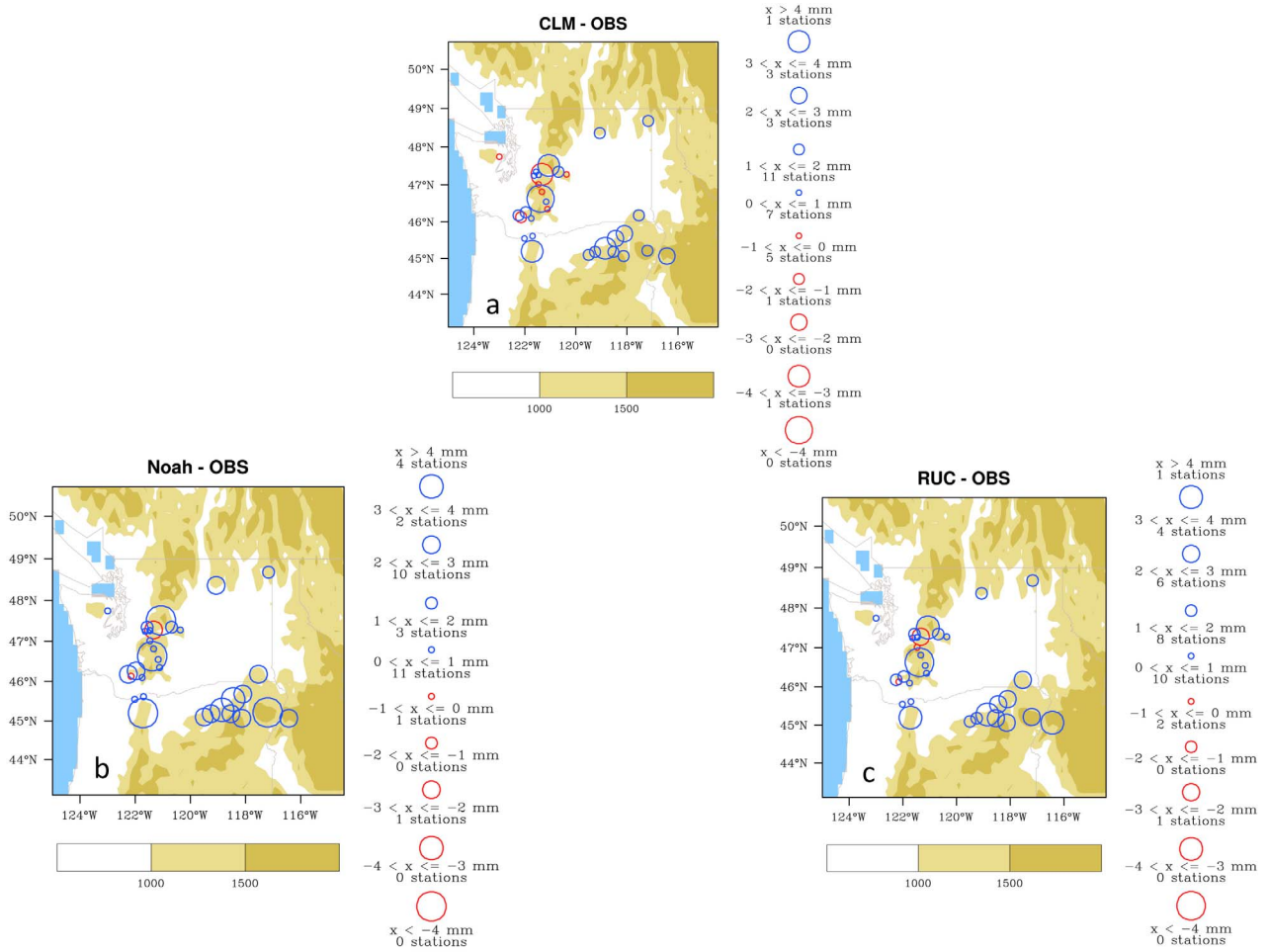

Figure 9. Same as Figure 3 except for precipitation.

distribution maps (Figure 9) show that in the CLM simulations there are seven stations where the bias is greater than 2 mm/d (Figure 9a), while in the Noah and RUC simulations, such stations are 16 and 11 mm/d, respectively. The CLM reduces the overestimated precipitation to some extent. Apparently, this reduction results largely from the lower evaporation in CLM (30 Wm^{-2}) as compared to that in Noah (63 Wm^{-2}) and RUC (49 Wm^{-2}) (Table 3). The lower evaporation is obviously attributable to the colder surface (4.1°C) in CLM due to the longer snow duration as compared to those in Noah and RUC. Although the surface skin temperatures in Noah and RUC are very close (5.2°C and 5.3°C, respectively), their evaporation shows a large difference. Further examination of these two models indicates that a wetter soil in Noah is found, where the volumetric soil moisture for a depth of 1 m is 0.36, averaged over the 32 SNOTEL stations for the period of 2 March through 30 June, but it is 0.18 in RUC (not shown). *Jin et al.* [2003] indicated that soil moisture calculation is strongly model dependent, and in this study, the soil moisture scheme of Noah produces a wetter soil than that of RUC.

[26] All three land surface schemes with WRF produce a higher surface air temperature at a height of 2 m than the observed value averaged over the 32 SNOTEL stations for the study period (Figure 10 and Table 2), and the averaged biases over those stations for CLM, Noah, and RUC are 0.6°C, 0.9°C, and 1.6°C for the period of 2 March through 30 June 2002. In the box plot of the temperature RMSE (Figure 11), the error box is in the lowest position for CLM, for which its 25% quartile is 2.4°C (2.6°C for Noah and 2.9°C for RUC). In the bias spatial maps, the number of stations with a bias greater than 1°C is 10 for CLM, 14 for Noah, and 21 for RUC. It is clear that CLM produces the best result among the three land surface models in temperature simulations. The 2 m height temperature is a function of surface skin temperature and sensible heat flux. Although the surface skin temperatures are close in Noah and RUC, the stronger sensible heat flux in RUC (61 Wm^{-2}) produces a higher 2 m height temperature (5.1°C) than that in Noah (40 Wm^{-2} and 4.4°C) (Table 3). Sensible heat flux in CLM

Table 3. The Mean Simulations From WRF With CLM, Noah, and RUC Over the 32 SNOTEL Stations for 2 March 2 Through 30 June 2002[a]

	CLM	Noah	RUC
TS (°C)	4.1	5.2	5.3
ALB (fraction)	0.25	0.20	0.17
SHX (Wm^{-2})	56	40	61
LHX (Wm^{-2})	30	63	49

[a]TS, surface skin temperature; ALB, albedo; SHX, sensible heat flux; LHX, latent heat flux.

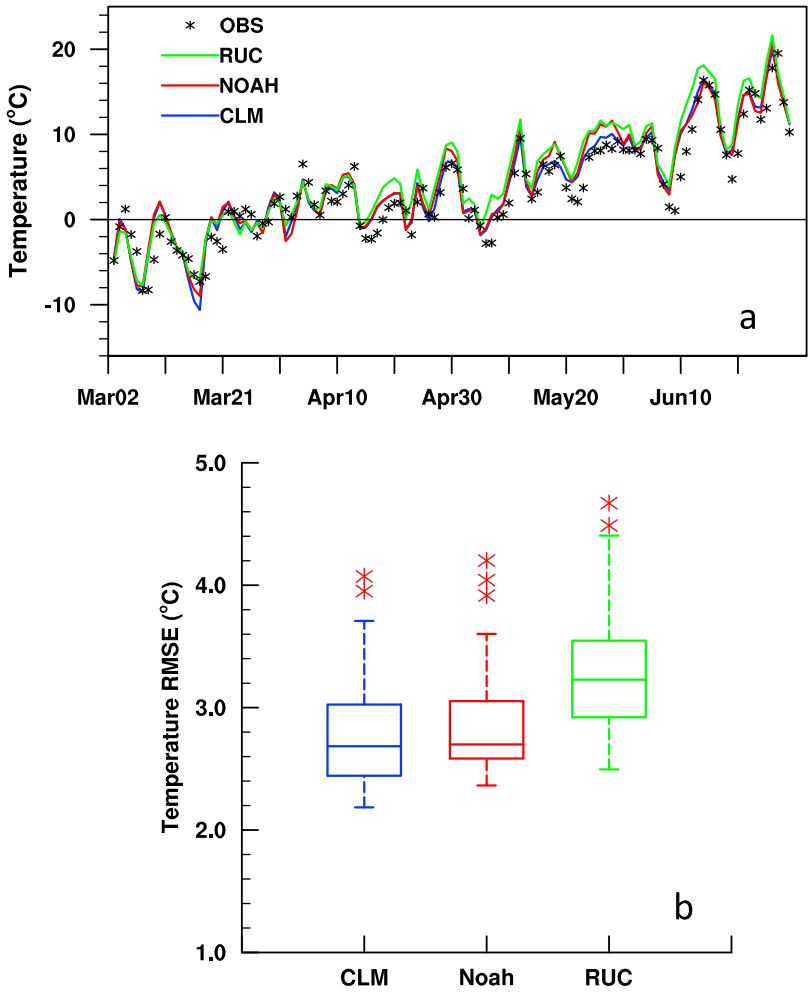

Figure 10. Same as Figure 8 except for temperature.

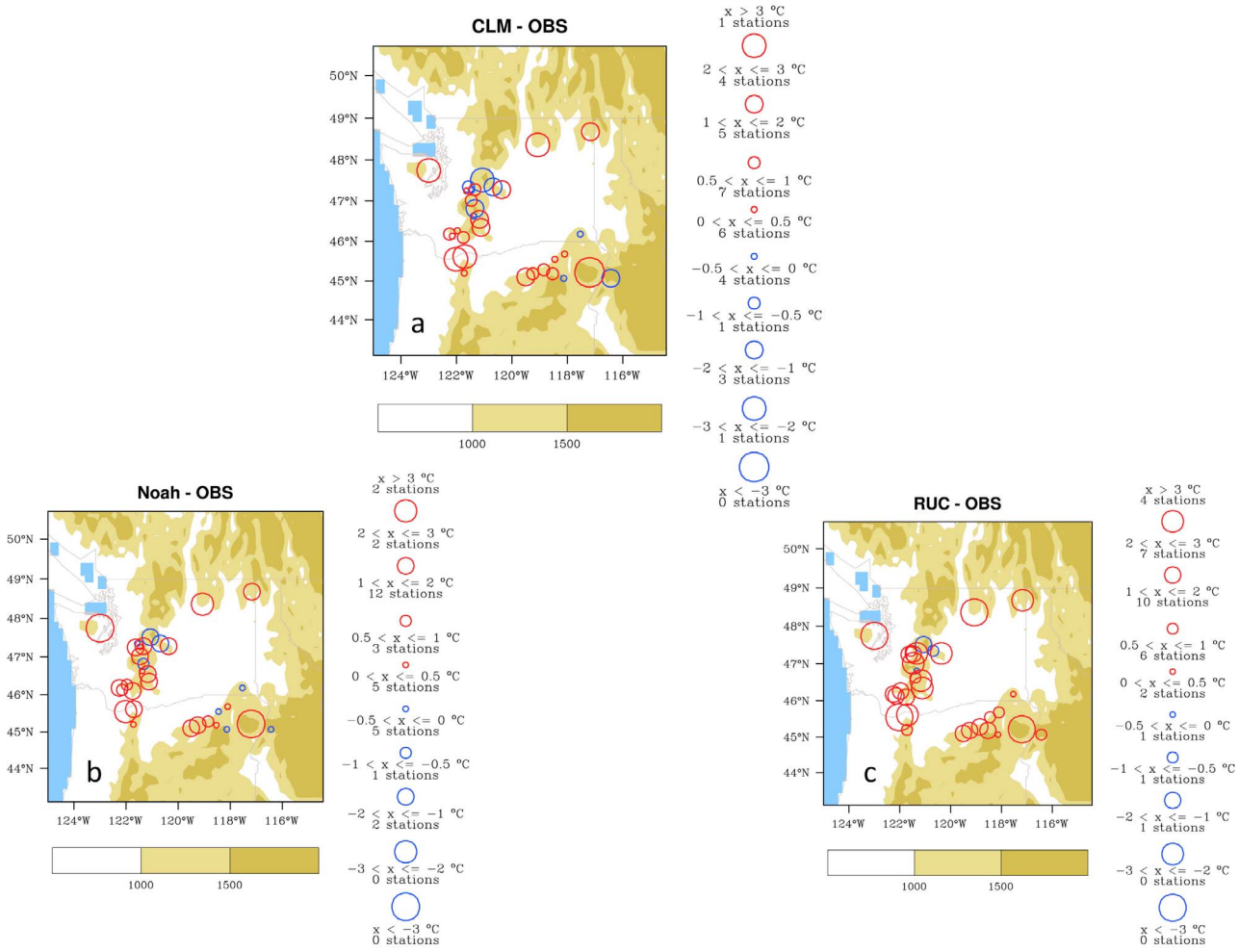

Figure 11. Same as Figure 3 except for temperature.

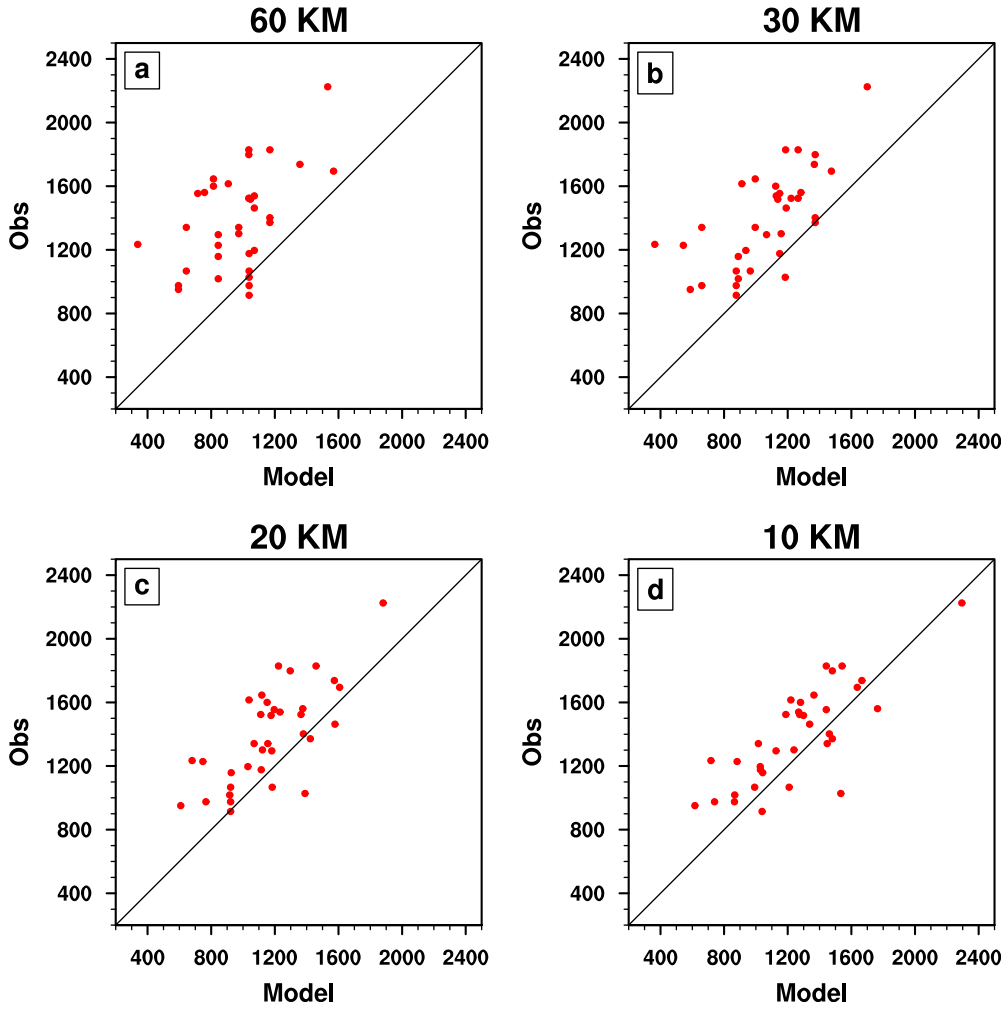

Figure 12. The actual elevations (vertical axis) versus the model elevations (horizontal axis) over the 32 SNOTEL stations (red dots) at (a) 60 km, (b) 30 km, (c) 20 km, and (d) 10 km.

(56 Wm^{-2}) is also higher than in Noah, but CLM's surface skin temperature was the lowest (4.1°C) among the three land surface models. The combination of the surface skin temperature and sensible heat flux in CLM produces the lowest 2 m height temperature (4.1°C) (Table 2), and this simulated temperature is closest to the observed value (3.5°C).

3.5. Topographic Impact on Snow Simulations

[27] In the WUS, seasonal snow is seen mostly at middle to high elevations. However, global weather and climate models are often unable to realistically simulate the WUS snow. One of the reasons is that the prescribed terrain elevations in these models cannot accurately reflect the reality due to their coarse resolutions. It is unclear that what spatial horizontal resolution would be adequate to reasonably simulate snow and related processes especially over regions of complex terrain such as the WUS. Figure 12 shows the scattering points for the observed elevations versus those prescribed in the WRF model over the 32 SNOTEL stations at different spatial resolutions (from 10 km to 60 km). The three land surface models use exactly the same terrain data obtained from the USGS. At 60 km resolution, the averaged elevation in the WRF model over the SNOTEL stations is 438 m lower than the actual value, and the root-mean-square error (RMSE) is 510 m (Table 4). With increasing the model resolution from 60 km to 10 km, both the bias and RMSE decrease.

[28] Table 4 indicates that the averaged model elevation over the SNOTEL stations is lower than the actual value at all four resolutions. In addition to the 30–10 km nested runs, additional WRF runs with CLM at different horizontal spatial resolutions were performed to examine how model resolution affects SWE, precipitation, and temperature simulations. These additional runs were 180–60 km, 90–30 km, and 60–20 km nested WRF-CLM simulations. The SWE simulations

Table 4. The Biases and Root-Mean-Square Errors Between the Model and Actual Elevations at Different Spatial Resolutions Over the 32 SNOTEL Stations

	RMSE (m)	Bias (m)
60 km	510	428
30 km	402	329
20 km	312	225
10 km	248	139

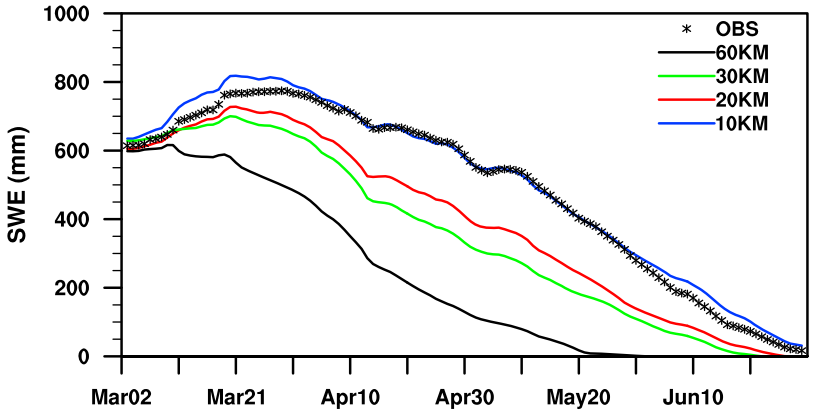

Figure 13. The SWE observations and simulations with WRF-CLM at different resolutions averaged over the 32 SNOTEL stations for the period of 2 March through 30 June 2002.

from the inner domains at the different resolutions (10 km, 20 km, 30 km, and 60 km) are shown in Figure 13. It seen that the simulated SWE agrees best with the observation at 10 km resolution, while the model underestimates SWE at those resolutions coarser than 10 km. In addition, the WRF-CLM slightly overestimates surface air temperature at 10 km resolution at a height of 2 m with a bias of 0.6°C (Table 5), as discussed above, but the WRF-CLM produces the highest bias (4.2°C) at the resolution of 60 km averaged over the SNOTEL stations, where the model also has the largest RMSE and bias in elevation. Table 5 shows that the averaged temperature decreases with an increase in the resolution from 60 km to 10 km, which is most likely linked to an environmental lapse rate and a feedback from the thicker SWE values. However, precipitation increases when the resolution increases from 60 km to 10 km, which is possibly triggered by the steeper terrain at the higher resolutions. It is apparent that the lowest precipitation bias occurs at 20 km resolution, but the best snow simulation is seen at 10 km resolution. However, these results are not contradictory. Our study period is focused mostly on the snowmelt season in which precipitation falls largely as rain. During this period of time, the vulnerability of the SWE simulations to the simulated precipitation bias is reduced, although precipitation could still bring energy to the snowpack and change its melting pattern. However, such a pattern change is not explicitly seen in our simulation cases. Although further increases in the model resolution can reduce the RMSE and bias in elevation, they may not provide additional benefits to the SWE simulations, which are a major focus of this study.

[29] In order to further identify the impact of the elevation on SWE simulations in our study region, one more WRF-CLM simulation is carried out with 60–20 km nested domains. In this simulation, all the other modeling settings are the same as those for the previous 60–20 km nested simulations, but the elevations at the 32 SNOTEL stations are replaced with the observed values as show in Figure 12. Figure 14 indicates that such a replacement dramatically improves the SWE simulation, which is 499 mm on average over the study period from 2 March through 30 June 2002, when compared to the observed value of 494 mm. At the same time, the temperature bias is only 0.1°C, while the precipitation bias is 0.9 mm/d. The precipitation bias for the new 20 km resolution simulations is comparable to that from the original model run at the same resolution, but the temperature bias is markedly reduced from 0.6°C to 0.1°C, resulting in a significant improvement of the SWE simulation. This improvement implies that temperature played a more dominant role in SWE simulations during our study period and indicates that a realistic topography in WRF is a vital to SWE, temperature, and precipitation simulations.

4. Conclusions and Discussions

[30] The objective of this study is to better understand and improve snow simulations at regional scales by coupling a sophisticated snow model with a next generation regional climate model. The results indicate that the snow simulations are dramatically improved with this newly coupled model. Further analysis shows that such an improvement results from more realistic allocation of surface energy in the new land surface model when compared to that in the two land surface schemes embedded in the release version of WRF. Meanwhile, the improved snow simulations further reduce the overestimated precipitation and warm biases that occur when WRF is coupled with Noah and RUC. The reduction in precipitation is caused by lower surface evaporation in CLM due to its colder surface resulting from the longer, more realistic snow duration. The alleviated warm bias is also related to snow simulations that are more accurate than those in WRF coupled with Noah and RUC.

[31] Our simulations also indicate that canopy sheltering effects play an important role in snowmelt when the peak SWE is low (e.g., <900 mm). Without considering these

Table 5. The Biases of the WRF-CLM Simulations at Different Spatial Resolutions Over the 32 SNOTEL Stations for 2 March Through 30 June 2002[a]

	SWE (mm)	Temperature (°C)	Precipitation (mm/d)
10 km	17	0.6	1.1
20 km	−103	1.5	0.3
30 km	−144	2.2	−0.7
60 km	−267	4.2	−1.0
20 km ht[a]	5	0.1	0.9

[a]Represents the simulations where the actual elevations are used over the 32 SNOTEL stations.

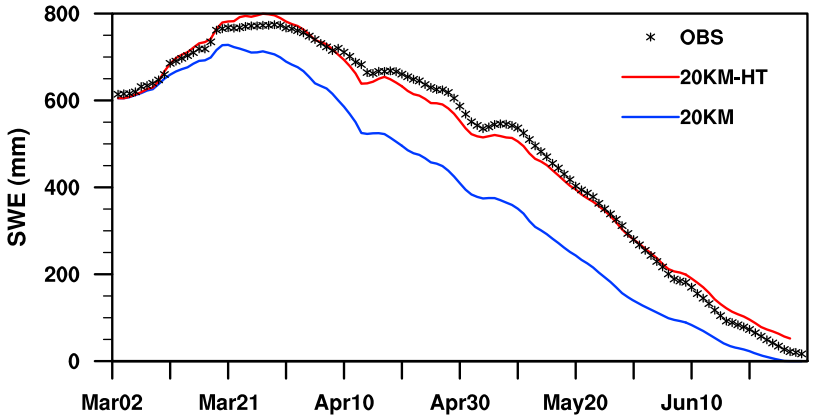

Figure 14. The SWE observations and simulations with WRF-CLM at 20 km resolution averaged over the 32 SNOTEL stations for the period of 2 March through 30 June 2002. The red line represents the SWE simulations where the model elevations at the 32 SNOTEL stations were replaced with the actual elevations.

effects, our model will produce a faster snowmelt than the observation for low peak SWEs. However, the canopy sheltering effects are not obviously seen when the peak SWE is high (e.g., >900 mm). The high albedo induced by this high peak SWE will result in weak solar radiation absorption, which can be approximately analogous to the reduced surface net solar radiation due to the sheltering effects. However, the modeling results need to be further verified with more observations, which are currently not available in our study region.

[32] Additional WRF runs show that topography plays an important role in snow simulations in our study area. WRF with CLM at 10 km resolution produces the most accurate SWE simulations as compared to the simulations at coarser resolutions where SWE is underestimated. However, WRF-CLM generates realistic SWE simulations at 20 km resolution when the model elevations at our selected SNOTEL stations over the Columbia River Basin are replaced with the observed values, further indicating the importance of topography to SWE simulations. These simulations also indicate that temperature plays a more dominant role than precipitation in SWE simulations during the snowmelt season.

[33] It is evident that WRF still overestimates precipitation in this mountainous area when a more realistic land surface model is coupled with it. This overestimation could generate higher snowpack especially during snow accumulation seasons. Atmospheric processes and related parameterizations such as microphysics or convection could contribute to overestimated precipitation. Future model calibration and validation with observed atmospheric processes are needed to achieve better precipitation simulations, and multiyear simulations over different snow-dominant regions are also necessary for further model evaluation. In general, this study shows that the coupled WRF-CLM significantly improves simulations of snow and related processes over the selected SNOTEL stations, and this improved version of WRF provides an important tool for regional weather, climate and water resources research and forecasts.

[34] **Acknowledgments.** This work was supported by the Utah Agricultural Experiment Station, EPA RD83418601, and the NOAA MAPP NA090AR4310195 grant.

References

Andreadis, K., P. Storck, and D. P. Lettenmaier (2009), Modeling snow accumulation and ablation processes in forested environments, *Water Resour. Res.*, *45*, W05429, doi:10.1029/2008WR007042.

Barlage, M., F. Chen, M. Tewari, K. Ikeda, D. Gochis, J. Dudhia, R. Rasmussen, B. Livneh, M. Ek, and K. Mitchell (2010), Noah land surface model modifications to improve snowpack prediction in the Colorado Rocky Mountains, *J. Geophys. Res.*, *115*, D22101, doi:10.1029/2009JD013470.

Bonan, G. B., K. W. Oleson, M. Vertenstein, S. Levis, X. Zeng, Y. Dai, R. E. Dickinson, and Z.-L. Yang (2002), The land surface climatology of the Community Land Model coupled to the NCAR Community Climate Model, *J. Clim.*, *15*, 3123–3149, doi:10.1175/1520-0442(2002)015<3123:TLSCOT>2.0.CO;2.

Chen, F., and J. Dudhia (2001), Coupling an advanced land-surface/hydrology model with the Penn State/NCAR MM5 modeling system. Part I: Model implementation and sensitivity, *Mon. Weather Rev.*, *129*, 569–585, doi:10.1175/1520-0493(2001)129<0569:CAALSH>2.0.CO;2.

Chou, M.-D., and M. J. Suarez (1999), A solar radiation parameterization for atmospheric studies, *NASA Tech. Memo.*, *NASA TM-1999-104606*, vol. 15, 40 pp.

Dickinson, R. E. (1983), Land surface processes and climate—Surface albedos and energy balance, *Adv. Geophys.*, *25*, 305–353, doi:10.1016/S0065-2687(08)60176-4.

Grant, L. O., and A. M. Kahan (1974), Weather modification for augmenting orographic precipitation, in *Weather and Climate Modification*, edited by W. N. Hess, pp. 282–317, John Wiley, New York.

Grell, G. A., and D. Dévényi (2002), A generalized approach to parameterizing convection combining ensemble and data assimilation techniques, *Geophys. Res. Lett.*, *29*(14), 1693, doi:10.1029/2002GL015311.

Hong, S.-Y., J. Dudhia, and S.-H. Chen (2004), A revised approach to ice microphysical processes for the bulk parameterization of clouds and precipitation, *Mon. Weather Rev.*, *132*, 103–120, doi:10.1175/1520-0493(2004)132<0103:ARATIM>2.0.CO;2.

Howat, I. M., and S. Tulaczyk (2005), Trends in spring snowpack over a half-century of climate warming in California, USA, *Ann. Glaciol.*, *40*, 151–156, doi:10.3189/172756405781813816.

Intergovernmental Panel on Climate Change (2008), *Climate Change 2007: Synthesis Report*, 104 pp., Intergov. Panel on Clim. Change, Geneva, Switzerland.

Janjic, Z. I. (1996), The Mellor-Yamada level 2.5 scheme in the NCEP Eta Model, paper presented at 11th Conference on Numerical Weather Prediction, Am. Meteorol. Soc., Norfolk, Va.

Jin, J., and N. L. Miller (2007), Analysis of the impact of snow on daily weather variability in mountainous regions using MM5, *J. Hydrometeorol.*, *8*, 245–258, doi:10.1175/JHM565.1.

Jin, J., X. Gao, Z.-L. Yang, R. C. Bales, S. Sorooshian, R. E. Dickinson, S.-F. Sun, and G.-X. Wu (1999a), Comparative analyses of physically based snowmelt models for climate simulations, *J. Clim.*, *12*, 2643–2657, doi:10.1175/1520-0442(1999)012<2643:CAOPBS>2.0.CO;2.

Jin, J., X. Gao, S. Sorooshian, Z.-L. Yang, R. C. Bales, R. E. Dickinson, S.-F. Sun, and G.-X. Wu (1999b), One-dimensional snow water and

energy balance model for vegetated surfaces, *Hydrol. Processes*, *13*, 2467–2482, doi:10.1002/(SICI)1099-1085(199910)13:14/15<2467::AID-HYP861>3.0.CO;2-J.

Jin, J., X. Gao, and S. Sorooshian (2003), Impact of model calibration on high-latitude land-surface processes: PILPS 2(e) calibration/validation experiments, *Global Planet. Change*, *38*, 73–80, doi:10.1016/S0921-8181(03)00006-7.

Jin, J., N. L. Miller, S. Sorooshian, and X. Gao (2006), Relationship between atmospheric circulation and snowpack in the western USA, *Hydrol. Processes*, *20*, 753–767, doi:10.1002/hyp.6126.

Jin, J., N. L. Miller, and N. Schegel (2010), Sensitivity study of four land surface schemes in the WRF model, *Adv. Meteorol.*, *2010*, 167436, doi:10.1155/2010/167436.

Knowles, N., M. D. Dettinger, and D. R. Cayan (2006), Trends in snowfall versus rainfall in the western United States, *J. Clim.*, *19*, 4545–4559, doi:10.1175/JCLI3850.1.

LeMone, M. A., F. Chen, M. Tewari, J. Dudhia, B. Geerts, Q. Miao, R. L. Coulter, and R. L. Grossman (2010a), Simulating the IHOP_2002 fair-weather CBL with the WRF-ARW-Noah modeling system. Part I: Surface fluxes and CBL structure and evolution along the eastern track, *Mon. Weather Rev.*, *138*, 722–744, doi:10.1175/2009MWR3003.1.

LeMone, M. A., F. Chen, M. Tewari, J. Dudhia, B. Geerts, Q. Miao, R. L. Coulter, and R. L. Grossman (2010b), Simulating the IHOP_2002 fair-weather CBL with the WRF-ARW-Noah modeling system. Part II: Structures from a few kilometers to 100 km across, *Mon. Weather Rev.*, *138*, 745–764, doi:10.1175/2009MWR3004.1.

Leung, L. R., and Y. Qian (2003), The sensitivity of precipitation and snowpack simulations to model resolution via nesting in regions of complex terrain, *J. Hydrometeorol.*, *4*, 1025–1043, doi:10.1175/1525-7541(2003)004<1025:TSOPAS>2.0.CO;2.

Livneh, B., Y. Xia, K. E. Mitchell, M. B. Ek, and D. P. Lettenmaier (2010), Noah LSM snow model diagnostics and enhancements, *J. Hydrometeorol.*, *11*, 721–738, doi:10.1175/2009JHM1174.1.

Lo, F., and P. M. Clark (2002), Relationships between spring snow mass and summer precipitation in the southwestern United States associated with the North American monsoon system, *J. Clim.*, *15*, 1378–1385, doi:10.1175/1520-0442(2002)015<1378:RBSSMA>2.0.CO;2.

McCabe, G. J., and P. M. Clark (2005), Trend and variability in snowmelt runoff in the western United States, *J. Hydrometeorol.*, *6*(4), 476–482, doi:10.1175/JHM428.1.

McCabe, G. J., and M. D. Dettinger (2002), Primary modes and predictability of year-to-year snowpack variations in the western United States from teleconnections with Pacific Ocean climate, *J. Hydrometeorol.*, *3*, 13–25, doi:10.1175/1525-7541(2002)003<0013:PMAPOY>2.0.CO;2.

McCabe, G. J., and D. M. Wolock (1999), General-circulation-model simulations of future snowpack in the western United States, *J. Am. Water Resour. Assoc.*, *35*, 1473–1484, doi:10.1111/j.1752-1688.1999.tb04231.x.

McKeen, S., et al. (2005), Assessment of an ensemble of seven real-time ozone forecasts over eastern North America during the summer of 2004, *J. Geophys. Res.*, *110*, D21307, doi:10.1029/2005JD005858.

Mlawer, E. J., S. J. Taubman, P. D. Brown, M. J. Iacono, and S. A. Clough (1997), Radiative transfer for inhomogeneous atmosphere: RRTM, a validated correlated-k model for the longwave, *J. Geophys. Res.*, *102*(D14), 16,663–16,682, doi:10.1029/97JD00237.

Mote, P. W. (2003), Trends in snow water equivalent in the Pacific Northwest and their climatic causes, *Geophys. Res. Lett.*, *30*(12), 1601, doi:10.1029/2003GL017258.

Niu, G.-Y., and Z.-L. Yang (2007), An observation-based formulation of snow cover fraction and its evaluation over large North American river basins, *J. Geophys. Res.*, *112*, D21101, doi:10.1029/2007JD008674.

Oleson, K. W., et al. (2004), Technical description of the community land model (CLM), *NCAR Tech. Note NCAR/TN-461+STR*, 186 pp., Natl. Cent. for Atmos. Res., Boulder, Colo.

Pan, H.-L., and L. Mahrt (1987), Interaction between soil hydrology and boundary-layer development, *Boundary Layer Meteorol.*, *38*, 185–202, doi:10.1007/BF00121563.

Pan, M., et al. (2003), Snow process modeling in the North American Land Data Assimilation System (NLDAS): 2. Evaluation of model simulated snow water equivalent, *J. Geophys. Res.*, *108*(D22), 8850, doi:10.1029/2003JD003994.

Rauscher, S. A., J. S. Pal, N. S. Diffenbaugh, and M. M. Benedetti (2008), Future changes in snowmelt-driven runoff timing over the western US, *Geophys. Res. Lett.*, *35*, L16703, doi:10.1029/2008GL034424.

Sellers, P. J. (1985), Canopy reflectance, photosynthesis and transpiration, *Int. J. Remote Sens.*, *6*, 1335–1372, doi:10.1080/01431168508948283.

Serreze, M. C., M. P. Clark, R. L. Amstrong, D. A. McGinnis, and R. S. Pulwarty (1999), Characteristics of western United States snowpack from snowpack telemetry (SNOTEL) data, *Water Resour. Res.*, *35*, 2145–2160, doi:10.1029/1999WR900090.

Smirnova, T. G., J. M. Brown, and S. G. Benjamin (1997), Performance of different soil model configurations in simulating ground surface temperature and surface fluxes, *Mon. Weather Rev.*, *125*, 1870–1884, doi:10.1175/1520-0493(1997)125<1870:PODSMC>2.0.CO;2.

Smirnova, T. G., J. M. Brown, S. G. Benjamin, and D. Kim (2000), Parameterization of cold-season processes in the MAPS land-surface scheme, *J. Geophys. Res.*, *105*(D3), 4077–4086, doi:10.1029/1999JD901047.

Subin, Z. M., W. J. Riley, J. Jin, D. S. Christianson, M. S. Torn, and L. M. Kueppers (2011), Ecosystem feedbacks to climate change in California: Development, testing, and analysis using a coupled regional atmosphere and land-surface model (WRF3–CLM3.5), *Earth Interact.*, *15*, 1–38, doi:10.1175/2010EI331.1.

Sun, S.-F., J. Jin, and Y. Xue (1999), A simple snow-atmosphere-soil transfer model (SAST), *J. Geophys. Res.*, *104*(D16), 19,587–19,597, doi:10.1029/1999JD900305.

Wang, Z., X. Zeng, and M. Decker (2010), Improving snow processes in the Noah land model, *J. Geophys. Res.*, *115*, D20108, doi:10.1029/2009JD013761.

Zeng, X., M. Shaikh, Y. Dai, R. E. Dickinson, and R. Myneni (2002), Coupling of the common land model to the NCAR community climate model, *J. Clim.*, *15*, 1832–1854, doi:10.1175/1520-0442(2002)015<1832:COTCLM>2.0.CO;2.